# ChinaSoyArea10m: a dataset of soybean planting areas with a spatial resolution of 10 m across China from 2017 to 2021

Qinghang Mei[1,2,3], Zhao Zhang[1,2], Jichong Han[1,2,4], Jie Song[1,2,4], Jinwei Dong[5,6], Huaqing Wu[1,2,3], Jialu Xu[1,2], Fulu Tao[5,6]

[1] Joint International Research Laboratory of Catastrophe Simulation and Systemic Risk Governance,Beijing Normal University, Zhuhai 519087, China

[2] School of National Safety and Emergency Management, Beijing Normal University, Beijing 100875 / Zhuhai 519087, China

[3] Faculty of Geographical Science, Beijing Normal University, Beijing 100875, China

[4] School of Systems Science, Beijing Normal University, Beijing 100875, China

[5] Key Laboratory of Land Surface Pattern and Simulation, Institute of Geographical Sciences and Natural Resources Research, Chinese Academy of Sciences, Beijing, 100101, China

[6] College of Resources and Environment, University of Chinese Academy of Sciences, Beijing 100049, China

*Correspondence to*: Zhao Zhang (zhangzhao@bnu.edu.cn)

18    **Abstract**

19    Soybean, an essential food crop, has witnessed a steady rise in demand in recent years. There is a lack of

20    high-resolution annual maps depicting soybean planting areas in China, despite China being the world's

21    largest consumer and fourth largest producer of soybeans. To address this gap, we developed a novel

22    Regional Adaptation Spectra-Phenology Integration method (RASP) based on Sentinel-2 remote sensing

23    images from the Google Earth Engine (GEE) platform. We utilized various auxiliary data (e.g., cropland

24    layer, detailed phenology observations) to select the specific spectra and indices that differentiate

25    soybeans most effectively from other crops across various regions. These features were then input for an

26    unsupervised classifier (K-means), and the most likely type was determined by a cluster assignment

27    method based on dynamic time warping (DTW). For the first time, we generated a dataset of soybean

28    planting areas across China, with a high spatial resolution of 10 meters, spanning from 2017 to 2021

29    (ChinaSoyArea10m). The $R^2$ values between the mapping results and the census data at both county- and

30    prefecture-level were consistently around 0.85 in 2017-2020. Moreover, the overall accuracy of mapping

31    results at the field level in 2017, 2018, and 2019 were 77.08%, 85.16% and 86.77%, respectively.

32    Consistency with census data was improved at the county level ($R^2$ increased from 0.53 to 0.84),

33    compared to the existing 10-m crop-type maps in Northeast China (Crop Data Layer, CDL) based on

34    field samples and supervised classification methods. ChinaSoyArea10m is spatially consistent well with

35    the two existing datasets (CDL and GLAD maize-soybean map). ChinaSoyArea10m provides important

36    information for sustainable soybean production and management, as well as agricultural system modeling

37    and optimization. ChinaSoyArea10m can be downloaded from an open-data repository (DOI:

38    https://zenodo.org/doi/10.5281/zenodo.10071426, Mei et al., 2023).

39    **1 Introduction**

40    Soybean, one of the most important crops around the world, plays an important role in diet and livestock

41    breeding (Hartman et al., 2011). As the global demand for protein and meat increases, China's demand

42    for soybeans has been keeping rising nowadays. In the past decade, China has averagely accounted for

43    over 30% of the world's total soybean consumption (Liu and Fan, 2021). Despite being the fourth-largest

44 producer of soybeans after Brazil, the United States, and Argentina, China's self-sufficiency rate is low

45 (FAOSTAT, 2023; Wang et al., 2023). Given the rapid growth of demand and the shortages of domestic

46 supply due to lower yield and self-sufficiency, mapping soybean planting areas across China is crucial

47 for sustainable soybean production and management (Cui and Shoemaker, 2018; Liu et al., 2021).

48     Soybean planting area in some regions of China was mapped in previous studies (You et al., 2021;

49 Huang et al., 2022; Chen et al., 2023), but long-term soybean maps over all major producing areas in

50 China have not been available. A decision tree method based on phenological and near-infrared

51 reflectance differences was applied in the state of Parana in Brazil to produce corn-soybean maps with a

52 resolution of 500 m (Zhong et al., 2016). However, this study was limited to one state and a simple

53 planting pattern (including soybeans and corn only) at a medium resolution. The field size in China is

54 generally small, and 500 m-resolution maps will inevitably bring pixel mixing problem (Lowder et al.,

55 2016). More recently, 20-year soybean-corn maps with 30 m resolution across the US Midwest have been

56 generated by collecting a large number of samples and using green chlorophyll vegetation index (GCVI)

57 time series features, which is a large-scale, high-precision soybean mapping attempt (Wang et al., 2020).

58 Similarly, high-precision soybean maps in China were also made by collecting major crop samples and

59 utilizing spectral reflectance and vegetation indexes characteristics, for 2017-2019 in Northeast China

60 (You et al., 2021). Some studies have utilized unique canopy water content and chlorophyll content to

61 produce soybean maps in the three provinces of Northeast China from 2017 to 2021 (Huang et al., 2022).

62 Other studies made laudable efforts to craft a comprehensive national maize-soybean map for China in

63 2019 by combining field data and regression estimators (Li et al., 2023). However, these studies were

64 confined in some degrees because of the specific region or a single year, despite prior attempts to

65 accurately map soybean cultivation areas. Long-term annual soybean maps over mainly planting areas

66 in China with a higher spatial resolution have not been available so far.

67     Mapping crops by remote sensing can be categorized into four methods : 1) supervision classification

68 based on a large number of field samples or high quality training labels (Song et al., 2017; You et al.,

69 2021; Shangguan et al., 2022; Li et al., 2023); 2) developing some composite indexes based on the feature

70 bands and determining the binary classification using appropriate thresholds (Huang et al., 2022; Chen

71 et al., 2023; Zhou et al., 2023); 3) threshold segmentation based on prior knowledge such as phenology

72 or spectra (Zhong et al., 2016); 4) combining unsupervised classification with cluster assignment (Wang

73  et al., 2019; You et al., 2023). Supervision classification methods relied on ground samples heavily, while

74  the 2nd and 3rd methods are both based on reliable and accurate thresholds. However, mapping soybean

75  by these methods was mainly applied in small areas, very few covering over a larger region. Because of

76  sufficient field samples, supervision classification can achieve maps with a higher accuracy, which is

77  relatively mature method used widely. However, collecting sufficient field samples is extremely time,

78  money, and labor consumed, and unsuitable for long-term years over larger areas (Luo et al., 2022).

79  Furthermore, the threshold-based methods (the 2nd and 3rd) have been applied into large areas, however,

80  determining the thresholds will inevitably bring significant uncertainty, especially for the areas with high

81  heterogeneity in climate, environment, and planting patterns. Thus, these methods show low

82  reproducibility, further hindering their application across diverse geographic areas. As for mapping

83  soybean, it is still a big challenge due to their similar growth characteristics with many other summer

84  crops (Wang et al., 2020; Di Tommaso et al., 2021). The thresholds that work well in some areas did not

85  perform well in other areas (Graesser and Ramankutty, 2017; Guo et al., 2018). These limitations restrict

86  accurate soybean maps available, especially over large regions in China. Given the challenges of

87  collecting sufficient field samples over larger region and the limited adaptability to environmental

88  variations of threshold-based method, previous researches have yet to achieve multi-year, high-resolution

89  soybean maps nationwide.

90  Along this line, the adaptive classification approach tailored to distinct areas, i.e., method (4), is a

91  highly effective for accurately mapping crops over a larger region. Such unsupervised classification can

92  effectively address the above issues such as insufficient samples and limited spatial scalability by training

93  classifiers separately in different areas (Ma et al., 2020; Wang et al., 2022). Remarkable successes have

94  been achieved when applying the approach into the United States in mapping soybean and maize (Wang

95  et al., 2019). Due to the different climatic and environmental conditions, together with huge differences

96  in cultivating patterns over various areas, crop phenological information has become an important

97  reference for crop classification. For example, the phenological observations at the agricultural

98  meteorological stations were employed as a reference to detect the critical phenological dates of pixels

99  through inflexion- and threshold-based methods, thereby generating planting areas for three major crops

100 in China with $R^2$ greater than 0.8 compared to county statistics (Luo et al., 2020). The time-weighted

101 dynamic time warping method based on the similarity of phenological curves of Normalized Difference

102 Vegetation Index (NDVI) has successfully estimated the planting area of maize in China, with provincial

103 averages for producer's and user's accuracies at 0.76 and 0.82, respectively (Shen et al., 2022).

104 Phenological-based Vertical transmit Horizontal receive (VH) polarized time series accurately captured

105 temporal characteristics of soybeans, thus were used for an unsupervised classifier to map the seasonal

106 soybeans, achieving an overall accuracy over 80% in Ujjain district (Kumari et al., 2019). By integrating

107 unsupervised classification's regional scalability with specific local soybean growth signs from

108 phenological data, we fully leverage soybean's characteristic spectra and vegetation indices during key

109 growth periods across different areas. Through training the local unsupervised classifier to accommodate

110 the crop growth variability across regions, and avoiding extensive jobs on collecting samples, the

111 approach provides an effective solution for regional adaptive large-area crop mapping.

112     The main objectives of this study are: 1) to develop a novel framework to map soybean planting area

113 over a larger region; 2) to test the generalization ability of the framework and assess the accuracy of maps

114 at different levels; and 3) to provide a new data product of soybean planting area across mainly planting

115 areas in China, for multi-years with a high spatial resolution.

116 **2 Materials and methods**

117 **2.1 Study area**

118 We selected 14 major soybean producing provinces (including Chongqing Municipality) as study area,

119 which cover over 90% of the total planting area in China (National Bureau of Statistics of China, 2023)

120 (Fig. 1). The soybean planting areas were classified into four agro-ecological zones (AEZs) based on

121 their diverse geographical environment and planting habits, including Northeast single cropping eco-

122 region (NE, Zone I), Huang-Huai-Hai double cropping eco-region (HH, Zone II), Middle-Lower Yangtze

123 River double cropping eco-region (MLY, Zone III) and Southwest double cropping eco-region (SW, Zone

124 IV) (Wang and Gai, 2002). In particular, Zone I and Zone II are the main soybean producer in China,

125 accounting for more than 70% of the national soybean planting area.
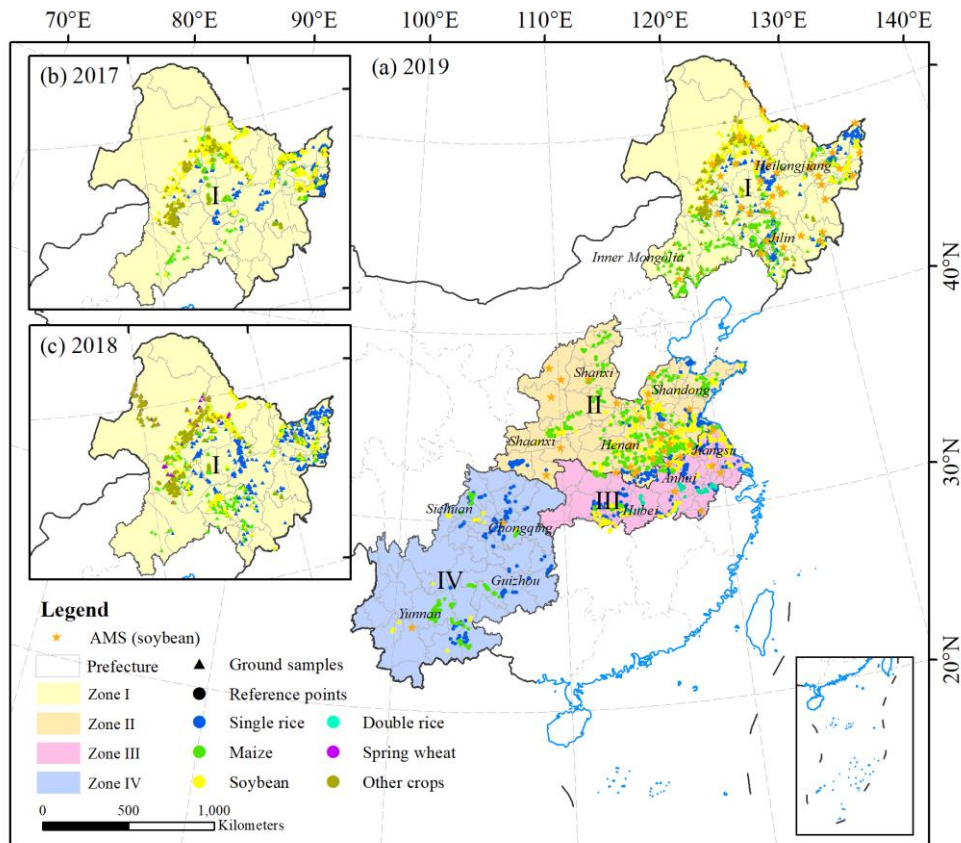
126

127 **Figure 1. The study area including 14 provinces (including Chongqing Municipality) and spatial distribution**

128 **of ground samples and reference points across China in (a) 2019, (b) 2017, and (c) 2018. The 14 provinces**

129 **include Heilongjiang, eastern Inner Mongolia, Anhui, Henan, eastern Sichuan, Jilin, Hubei, Guizhou, Jiangsu,**

130 **Yunnan, Shandong, Shaanxi, Shanxi, and Chongqing. Stars, triangles, and dots represent the locations of**

131 **soybean agricultural meteorological stations (AMSs), ground samples, and reference points, respectively.**

132 **2.2 Data**

133 **2.2.1 Remote sensing data**

134 We used Sentinel-2A/B Multi-Spectral Instrument (MSI) Level-1C top-of-atmosphere (TOA) reflectance

135 data during 2017-2021 (https://developers.google.com/earth-engine/datasets/catalog/COPERNICUS_S2,

136 last access: September 2023). Because of the longer-term coverage of Sentinel-2 Level-1C TOA

137 reflectance data, and the nearly identical spectral profile time series extracted from both products, we opt

138 to use L1C products instead of L2A, considering that TOA images fully meet the crop classification

139 requirements (You and Dong, 2020; Han et al., 2021; Luo et al., 2022). Sentinel-2 sensors provide

140 observations in 13 spectral bands at 10 m or 20 m resolution. The red-edge bands and shortwave infrared

141   bands equipped with sentinel-2 play a great role in enhancing the accuracy of crop classification (Luo et

142   al., 2021; Marshall et al., 2022). In addition, the S2 cloud probability dataset provided by the official can

143   identify cloud pollution areas and be used as cloud removal processing.

144   **2.2.2 In-situ phenological observations**

145   The soybean phenology observations in study area from 2017 to 2020 were obtained from 76 agricultural

146   meteorological stations (AMSs) governed by the CMA (https://data.cma.cn/, last access: May 2022).

147   Phenology information of each AMS is observed on alternate days or once a day, and key phenological

148   events such as sowing, emergence, three-true-leaves, branching, flowering, podding, full-seeding, and

149   maturity are noted by technicians to ensure accuracy. We defined the period from sowing to flowering as

150   the vegetative growth period (VGP), and the period from flowering to maturity as the reproductive

151   growth period (RGP) of soybeans (Gong et al., 2021). In cases of missing observation for a specific year,

152   we inserted the average of two closest observations before and after the year. For instance, if there was

153   missing data of flowering date in 2017, we filled it with the average of flowering records in 2016 and

154   2018 at the same station.

155   **2.2.3 Cropland data**

156   GLAD cropland product with a 30-m resolution in China was used as cropland masks

157   (https://glad.umd.edu/dataset/croplands, last access: September 2023) (Potapov et al., 2022). The crop

158   layer was conducted every four years from 2000 to 2019. We used the file for the 2016-2019 interval

159   which is closest to the study years. GLAD's overall accuracy of pixel-wise validation is 0.88 in China,

160   consistent well with the census data. The accuracy of the product is higher than that of similar products,

161   making it a reliable for crop mapping (Zhang et al., 2022).

162   **2.2.4 Census data and ground samples**

163   To determine the number of clusters at prefecture-level and validate the accuracy of the soybean maps at

164   county (2017-2018) or prefecture (2019-2020) level, we utilized agricultural census data obtained from

165   the statistical yearbook of each county or province by accessing National Bureau of Statistics of China

166   (http://www.stats.gov.cn/, last accessed: June 2023).

167   We used both ground samples and reference points based on available datasets to determine soybean

168  standard curves and assess the reliability of the soybean maps (Fig. 1). All points were randomly divided

169  in a 3:7 ratio for standard curve calculation and accuracy validation, respectively (Dong et al., 2020). We

170  collected ground samples from field surveys from 2017 to 2019 in Heilongjiang (HLJ), Inner Mongolia

171  (NMG), Anhui (AH), Henan (HN), and Jilin (JL), which account for more than 70% of the country's total

172  soybean planting area (Table 1). Crop types (soybean, maize, rice, wheat, others) and other land cover

173  types were recorded. To ensure the impartiality of verification results, we only selected crop samples for

174  validation. In provinces without ground samples, we manually selected reference points on large soybean

175  plots based on GLAD (https://glad.earthengine.app/view/china-crop-map, last access: March 2024)

176  soybean layer. The criterions selected are: (1) located in large plots; (2) false color composite image (R:

177  NIR, G: SWIR2, B: SWIR1) at the peak of growing season (Song et al., 2017; You and Dong, 2020); (3)

178  phenological characteristics similar to local observations. Additionally, the reference points of maize,

179  single-cropping rice and double-cropping rice in 2019 were selected based on GLAD maize layer, high

180  resolution single-season rice map (https://doi.org/10.57760/sciencedb.06963, last access: March 2024),

181  and double-season rice map (https://doi.org/10.12199/nesdc.ecodb.rs.2022.012, last access: March 2024)

182  with the same principle to explore the spectral characteristics of crops in each sub-zone of the studied

183  areas. The overall accuracy of all available maps in 2019 is above 85% (Pan et al., 2021; Li et al., 2023;

184  Shen et al., 2023).

185

**Table 1. Summary of ground samples for validation.**

|  |  | HLJ | NMG | AH | HN | JL |
|---|---|---|---|---|---|---|
| 2017 | Soybean | 1013 | 451 | - | - | 0 |
|  | Maize | 1061 | 146 | - | - | 11 |
|  | Rice | 513 | 38 | - | - | 13 |
|  | Other crops | 124 | 459 | - | - | 0 |
| 2018 | Soybean | 525 | 746 | 72 | 15 | 117 |
|  | Maize | 764 | 479 | 73 | 20 | 217 |
|  | Rice | 587 | 42 | 0 | 0 | 71 |
|  | Wheat | 10 | 141 | 0 | 0 | 0 |
|  | Other crops | 70 | 1069 | 0 | 0 | 0 |
| 2019 | Soybean | 901 | 562 | 51 | - | 26 |
|  | Maize | 468 | 463 | 53 | - | 197 |
|  | Rice | 392 | 36 | 0 | - | 148 |
|  | Other crops | 62 | 445 | 0 | - | 36 |

 **2.2.5 Existing products**

187 We utilized the crop map CDL of Northeast China from 2017 to 2019

188 ([https://figshare.com/articles/figure/The_10-m_crop_type_maps_in_Northeast_China_during_2017-](https://figshare.com/articles/figure/The_10-m_crop_type_maps_in_Northeast_China_during_2017-)

189 [2019/13090442](https://figshare.com/articles/figure/The_10-m_crop_type_maps_in_Northeast_China_during_2017-2019/13090442), last access: September 2023) for consistency comparison with census data, and the

190 2019 GLAD maize-soybean map as a reference for spatial detail comparison with ChinaSoyArea10m.

191 CDL is a 10m resolution crop map dataset of Northeast China from 2017 to 2019 that was created

192 using Sentinel-2 key spectral bands and vegetation indices, multi-year field samples, and random forest

193 classifiers (You et al., 2021). The maps include three crop types: rice, maize, and soybeans. The GLAD

194 maize-soybean Map is a national classification map for 2019 that was produced using random forests,

195 based on field surveys and area estimates (Li et al., 2023). The agreement ($R^2$) between GLAD and the

196 statistics is higher than 0.9, and the overall mapping accuracy is greater than 90%, making it a reliable

197 reference for comparing spatial details. We extracted the soybean layers from all the existing products.

198 **2.3 Methods**

199 Mapping soybean consists of three main steps (Fig.2): data processing, soybean mapping, and accuracy

200 assessment. It is important to note that the Regional Adaption Spectra-Phenology Integration (RASP)

201 soybean mapping strategy involves several key steps, including potential area identification, feature

202 selection, unsupervised learning, and cluster assignment. Finally, we conducted multi-comparisons

203 between our soybean products with others, including census data, ground samples, and existing datasets,

204 to evaluate the accuracy of our data product.
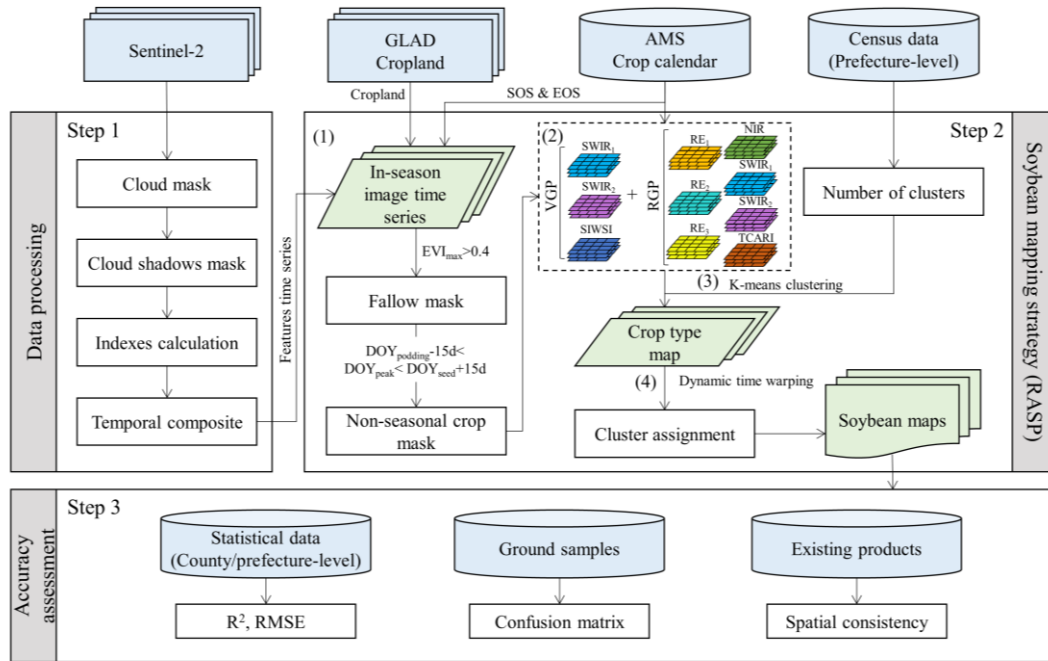
205

206 **Figure 2. The Regional Adaption Spectra-Phenology Integration methodology for retrieving soybean planting**

207 **area. AMS, agricultural meteorological station; $DOY_{podding}$, the podding date recorded by the nearest AMS;**

208 **EVI: Enhanced Vegetation Index; $DOY_{peak}$, the date when EVI reached peak; $DOY_{seed}$, the full-seed date**

209 **recorded by the nearest AMS; SOS, start of growing season; EOS, end of growing season; $SWIR_1$, Short Wave**

210 **Infrared band 1; $SWIR_2$, Short Wave Infrared band 2; SIWSI, shortwave Infrared Water Stress Index; $RE_1$,**

211 **Red Edge band 1; $RE_2$, Red Edge band 2; $RE_3$, Red Edge band 3; NIR, Near-infrared band; TCARI,**

212 **Transformed Chlorophyll Absorption in Reflectance Index; VGP: vegetative growing period; RGP:**

213 **reproductive growing season.**

214 **2.3.1 Data processing**

215 We employed the simple cloud score algorithm (Oreopoulos et al., 2011), QA60 band, cirrus band, and

216 cloud probability dataset to identify cloud masks. The following isolated cloud masks are created: (1)

217 Cloud and cirrus identified by QA60 band; (2) Cirrus identified by cirrus band in Level-1C products; (3)

218 Pixels with cloud score less than 0.9; and (4) Pixels with cloud probability more than 70. Each algorithm

219 has its own strengths and limitations. For example, QA60 band removes a large number of thin cirrus

220 clouds while ignoring small clouds with thicker resolution, and the fixed threshold values of cloud score

221 and cloud probability may introduce uncertainties. Therefore, we masked the pixels identified as clouds

222 by at least two methods to achieve better cloud removal effects. Then, we used Temporal Dark Outlier

223 Mask (TDOM) method to eliminate cloud shadows (Housman et al., 2018). We calculated the SIWSI

224 and TCARI indices based on the Sentinel-2 image set processed above (see 2.3.2(2)). To fill the data gaps

225 caused by cloud removal and smooth anomalies, Sentinel-2 time series was reconstructed by moving

226 median composite method, resulting in a 10-day interval composite time series. We set the half-window

227 size for the moving median methods to 10 days considering the 5-day revisit cycle of Sentinel-2 and

228 computational efficiency. In areas with notably limited clear observations, a gap-filling method was

229 conducted on the composite time series. This method involves substituting any given observation with

230 the median value from three neighboring observations (i.e., previous, current, and subsequent

231 observations) to maximize the continuity and completeness of time series.

**2.3.2 Regional Adaptation Spectra-Phenology Integration (RASP) soybean mapping strategy**

233 (1) Potential area identification

234 To minimize the impact from non-croplands, we firstly determine the potential cropping areas by

235 masking GLAD cropland layer over study area. Sentinel-2 images within growing season were extracted

236 by taking the sowing date and harvesting date recorded at the nearest agricultural meteorological station

237 (AMS) as the starting and ending dates of the growing season, respectively. Based on the cropland

238 extracted, we filtered out the pixels exhibiting an Enhanced Vegetation Index (EVI) maximum value

239 during the growing season less than 0.4 to remove fallow land according to the analysis of ground

240 samples (Fig. S1) and previous studies, which found that almost all crops had maximum EVI values

241 above 0.4 (Li et al., 2014; Zhang et al., 2017; Han et al., 2022). EVI is a vegetation index with high

242 sensitivity in biomass:

$$EVI = G \times \frac{\rho_{NIR} - \rho_{Red}}{\rho_{NIR} + C_1 \times \rho_{Red} - C_2 \times \rho_{Blue} + L} \tag{1}$$

243 Where $\rho_{NIR}$, $\rho_{Red}$, and $\rho_{Blue}$ represented the reflectance of the Near-infrared (835.1nm (S2A) / 833nm

244 (S2B)), Red (664.5nm (S2A) / 665nm (S2B)), Blue (496.6nm (S2A) / 492.1nm (S2B)), respectively.

245 The greenest period of soybean typically occurs between the podding date and the full-seed date, with a

246 difference of more than a month from the peak date of non-seasonal crops, such as wheat (Fig. 4a). We

247 obtained the phenological observations recorded by the nearest AMS as reference and set the restricted

248 time window from 15 days before the podding date ($DOY_{podding}$) to 15 days after the full-seed date

249 ($DOY_{seed}$) (Fig. 3). We generated the potential area by eliminating pixels whose EVI maximum occurs

250   outside the given time window because the phenological difference of soybeans in adjacent areas

251   generally does not exceed one month. Moreover, the impacts of cloud-covered pixels appearing in the

252   proposed period is minimized since we have reconstructed the original EVI time series.
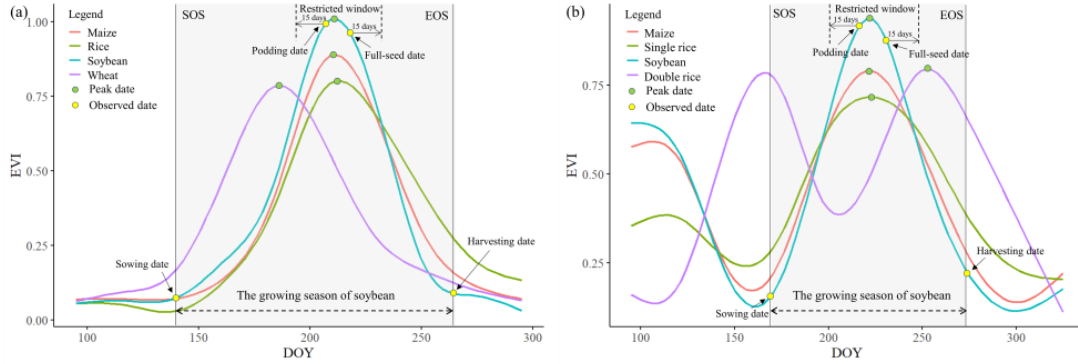
253

254   **Figure 3. Schematic diagram of seasonal crop identification for (a) single - and (b) double - cropping systems.**

255   (2) Feature selection

256   By exploring the spectral characteristics of crop field samples, we identified reflectance bands and

257   vegetation indices that are significantly associated with soybeans but different from other crops. We

258   selected six bands and two spectral indices for crop mapping, including Near-infrared (NIR) band, Red

259   edge band 1 (RE1), Red edge band 2 (RE2), Red edge band 3 (RE3), Short Wave Infrared band 1

260   (SWIR1), Short Wave Infrared band 2 (SWIR2), Shortwave Infrared Water Stress Index (SIWSI),

261   Transformed Chlorophyll Absorption in Reflectance Index (TCARI). SIWSI is an indicator of canopy

262   water content that reflects soil moisture variations and canopy water stress better than Normalized

263   Difference Vegetation Index (NDVI) (Fensholt and Sandholt, 2003; Olsen et al., 2015). TCARI is an

264   indicator which is sensitive to chlorophyll concentration (Sobejano-Paz et al., 2020). The two spectral

265   indices were calculated as follows:

$$SIWSI = \frac{\rho_{SWIR1} - \rho_{NIR}}{\rho_{SWIR1} + \rho_{NIR}} \tag{2}$$

$$TCARI = 3 \times ((\rho_{VRE1} - \rho_{Red}) - 0.2 \times (\rho_{VRE1} - \rho_{Green}) \times \rho_{VRE1}/\rho_{Red}) \tag{3}$$

266   Where $\rho_{SWIR1}$, $\rho_{NIR}$, $\rho_{VRE1}$, $\rho_{Red}$ and $\rho_{Green}$ represented the reflectance of the Short Wave Infrared

267   band1 (SWIR1, 1613.7nm (S2A) / 1610.4nm (S2B)), Near-infrared (835.1nm (S2A) / 833nm (S2B)),

268   Red Edge1 (VRE1, 703.9nm (S2A) / 703.8nm (S2B)), Red (664.5nm (S2A) / 665nm (S2B)), Green

269   (560nm (S2A) / 559nm (S2B)), respectively.

270   During early growing season of soybean (~DOY 120-190 in Zone I), the flooding signal of rice was

271   obvious due to the transplanting period. This resulted in a significantly lower SWIR reflectance and

272     SIWSI index for rice compared to those of soybean (Fig. 4f-h). SWIR bands and SIWSI index during the

273     vegetative growing period (VGP) of soybean can effectively distinguish dryland crops (such as soybean,

274     maize) from paddy crops (such as rice).

275     Soybean has a lower water content during the middle and later growing season (~DOY 190-220 in

276     Zone I) than maize, resulting in higher reflectivity in SWIR bands (Fig. 4b, 4f, 4g) (Chen et al., 2005). It

277     has been demonstrated that SWIR and red-edge bands can effectively differentiate soybean and maize

278     (Fig. 4c-g) (Zhong et al., 2016; You and Dong, 2020; Liu et al., 2018b). Additionally, the chlorophyll

279     content of soybean in the middle and late growth period was lower than that of maize, leading to

280     significantly higher TCARI values. Meanwhile, the timing of TCARI reaching saturation significantly

281     differs among soybean, rice, and wheat (Fig. 4i). All these spectral-phenological characteristics are also

282     applicable to soybeans planted in other sub-zones (Fig. S2-S4). Based on these findings, we selected NIR,

283     red-edge bands, short-wave infrared bands, and TCARI index during soybean reproductive growing

284     season (RGP) as key features.

285
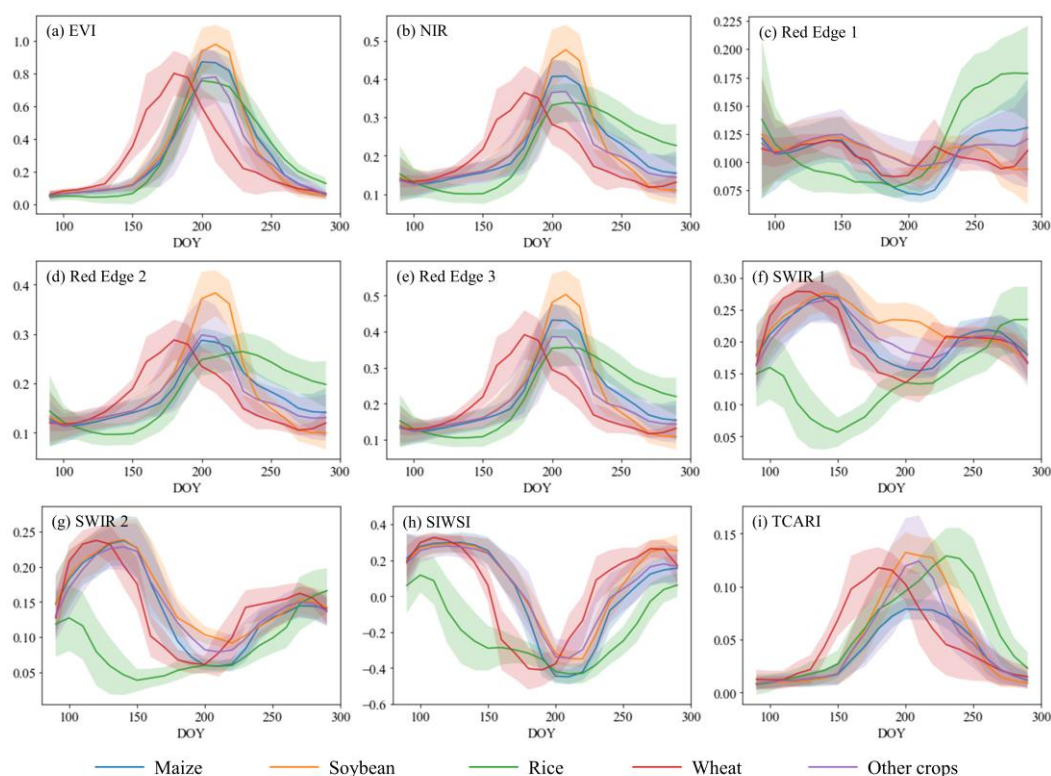
**Figure 4. Temporal profiles of (a-i) for major crops in Northeast China and (j) key soybean phenological periods by region based on ground samples. Lines depict the mean values of different crops and shaded areas depict error bars with one positive/negative standard deviation. The number at the bottom represents the key phenological periods of soybean: 1 – Sowing, 2 – Flowering, 3 – Seed fulling, 4 – Maturity.**

(3) Unsupervised learning

We utilized K-means algorithm to classify potential area data by using the wekaKMeans Clusterer provided by Google Earth Engine (GEE). The $m$ samples are divided into $k$ clusters by alternately assigning the samples to the nearest cluster centroid measured by Euclidean distance or the Manhattan distance and updating the cluster centroid to the mean of the samples assigned to the cluster. This approach had been widely used in land-cover classification and crop mapping (Xiong et al., 2017; Wang et al., 2019). We used the detailed phenological records at AMSs and selected the key phenological information as input features. The classifier was trained individually on each prefecture based on the number of clusters $k$ input. The cluster number $k$ is defined as the number of "major crops" that constituting 95% of the total area for seasonal crops (including rice, maize, soybean, cotton, peanuts, sesame, sweet potato, and sorghum) according to prefecture-level statistics, and plus one for "other crops".

(4) Cluster assignment

To identify the most likely cluster that represents soybean, we randomly selected 100 points per cluster and extracted feature series. We then used dynamic time warping (DTW) method to measure the similarity between each cluster's eight features involved in classification and the soybean standard curves. We averaged the data of 30% samples in each sub-zone to establish the standard curves, reducing the impact of regional phenological variations. The time coverage of Zone I-IV was set to April-September, May-October, June-October, and August-November, respectively, which are corresponding with the soybean growing season. The cluster with the minimal average DTW value was identified as the soybean cluster. DTW is a flexible algorithm that allows for deviations in time between two sequences, and it calculates the minimum distance between them by finding misalignment matches between elements. This approach is widely used in land cover and crop identification due to its ability to handle time distortions associated with seasonal changes (Guan et al., 2016; Dong et al., 2020).

### 2.3.3 Accuracy assessment

To assess the accuracy of the soybean maps we generated, we validated and compared the results using 1) county- and prefecture-level census data, 2) ground samples, and 3) existing products. Since the county-level statistics after 2019 were not fully collected, we used the county-level statistics for 2017-2018 and the prefecture-level statistics for 2019-2020 to calculate the $R^2$ and RMSE of the mapped area with the following equations:

$$R^2 = 1 - \frac{\sum_{i=1}^{n}(s_i - y_i)^2}{\sum_{i=1}^{n}(s_i - \bar{s})^2} \tag{4}$$

$$RMSE = \sqrt{\frac{\sum_{i=1}^{n}(s_i - y_i)^2}{n}} \tag{5}$$

where $s_i$ and $y_i$ are the statistical and mapped soybean area for county (prefecture) $i$, $\bar{s}$ is the average statistical area, and $n$ represents the total number of counties (prefectures). We calculated the local crop mapping area based on the Universal Transverse Mercator (UTM) projection corresponding to the location of the province.

We also used ground samples during 2017-2019 to verify the authenticity of the soybean maps. Confusion matrices were calculated as follows:

$$PA = \frac{N_i}{R_i} \tag{6}$$

$$UA = \frac{N_i}{C_i} \tag{7}$$

$$OA = \frac{N_c}{A} \tag{8}$$

$$F1 = 2 \times \frac{UA \times PA}{UA + PA} \tag{9}$$

where $N_i$ is the number of correctly identified validation samples of class $i$, $R_i$ is the number of ground validation samples of class $i$, $C_i$ is the number of validation samples classified as class $i$, $C_i$ is the number of validation samples classified as class $i$, $N_c$ is the total number of correctly identified validation samples, $A$ is the total number validation samples. $PA$, $UA$, and $OA$ represent producer's accuracy, user's accuracy, and overall accuracy, respectively.

To ensure that the products are accurate not only in quantity but also in space, we further compared the ChinaSoyArea10m with existing products in detail space.

**3 Results**

**3.1 Accuracy assessment**

We utilized the available census data from 2017-2020 (at county-level in 2017-2018 and prefecture-level in 2019-2020) to verify the accuracy of the soybean maps across the entire studied area. Annual ChinaSoyArea10m is consistent well with the census data ($R^2 > 0.8$), with an $R^2$ value of 0.84, 0.85, 0.82, and 0.86 for 2017, 2018, 2019, and 2020, respectively (Fig. 5). These results demonstrate that our RASP method is inter-annual robustness and can accurately capture annual dynamics of soybean planting areas. The scattered points are generally distributed around 1:1 line, without large overestimations or underestimations. However, the areas are overestimated for counties with planting area < 20 kha, or prefectures with planting area <100 kha (Fig. 5). This uncertainty, particularly overestimation, could be caused by the low proportion of soybean cultivation. If maize or other same-season crops are planted in a much higher proportion than soybeans there, distinctly recognizing soybeans (as a less prevalent crop) as a separate category will be a big challenge for classifiers, consequently resulting in misclassified clusters including maize or other crops.

The mapping accuracy in Zone I closely matched county-level statistics, showing high consistency ($R^2$=0.86). Zones II-IV also demonstrated reasonable agreement ($R^2$=0.50~0.69), despite relatively lower accuracy due to the scarcer planted areas (Fig. S5). No significant trend deviation from statistics was indicated for the mapping area in Zone I, with slight overestimates for Zone II and III, and underestimates for Zone IV (Fig. S5). These accuracy variations are acceptable, given the challenges in accurately identifying soybeans in regions where they are planted less prevalently. Specifically, maize is more dominant than soybeans in Zone II, while Zone III is characterized by diverse crops and complex planting patterns. Underestimation in Zone IV is possibly due to fewer clear observations in the southwest. Nevertheless, the overall accuracy across the zones is acceptable.

ChinaSoyArea10m is consistent well with census data compared to the existing product (CDL) (You et al., 2021), using both the county level in 2018 and prefecture level in 2019 (Fig. 6). CDL's results are consistent with census data at the prefecture scale, with more overestimations at the county level (Fig. 6), implying the comparison at finer scale would reveal more details. ChinaSoyArea10m is consistent

360    with statistics at the both levels ($R^2$ ~0.85), with $R^2$ increases 0.31 compared with CDL in county level

361    (Fig. 6a).
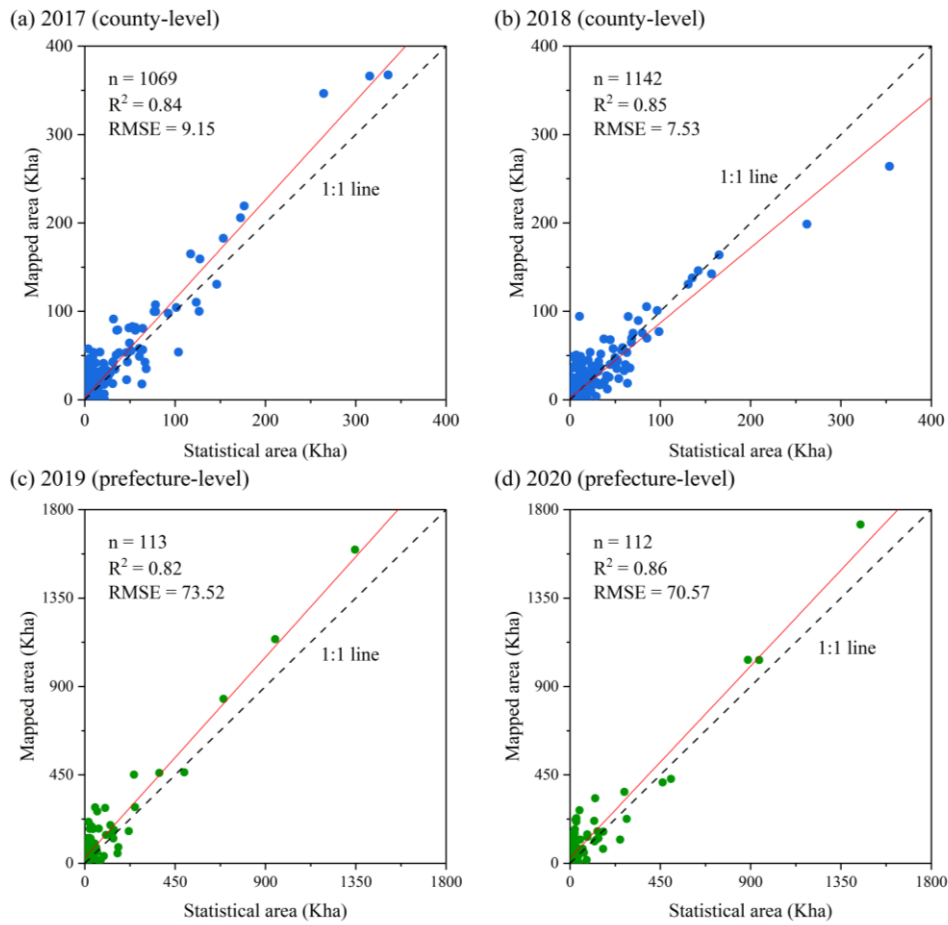
362

363    **Figure 5. Comparison of soybean areas with statistics in (a) 2017 at county-level, (b) 2018 at county-level, (c)**

364    **2019 at prefecture-level, (d) 2020 at prefecture-level.**
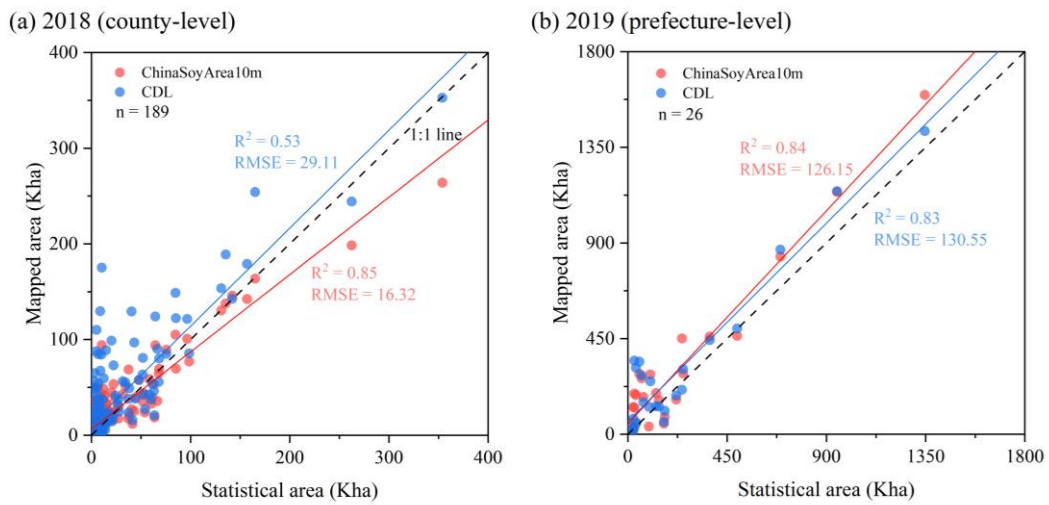
365

366    **Figure 6. Comparison of soybean areas of ChinaSoyArea10m and CDL with statistics in (a) 2018 at county-**

367    **level, (b) 2019 at prefecture-level.**

368    Furthermore, we used ground samples in 2017-2019 to validate the reliability of the soybean maps.

369    Since the soybean planting area maps are 0-1 binary images, we categorized the ground samples into

370    soybean and non-soybean (maize, rice, wheat, and other crops). The verification results based on ground

371    samples indicated that the overall accuracy of soybean maps during 2017-2019 was in the range of 77.08%

372    to 86.77%. The F1 scores of soybeans increased from 2017 to 2019 (0.69, 0.75 and 0.84, respectively)

373    (Table 2). The variance in accuracy among years could be attributed to the quality of Sentinel-2 images,

374    which had been indicated in previous studies (Liu et al., 2020; Han et al., 2021). The overall accuracy

375    for each sub-zone in 2019 varied from 83.58% to 90.67% (Table S1). Specifically, Zone I demonstrated

376    the highest producer's accuracy for soybean at 88.31%, aligning with its high consistency with statistics.

377    Zone III achieved the highest overall accuracy at 90.67%, attributed to its superior user's accuracy for

378    soybean, indicating fewer misclassifications, and effective differentiation from non-soybean crops (Table

379    S1). The producer's accuracy in Zone IV was relatively lower at 63.89%, possibly due to the limited

380    samples, high heterogeneity, and fewer clear observations (Table S1).

381    **Table 2. Confusion matrix of the soybean maps during 2017-2019.**

|  |  | Reference Map Soybean | Non-Soybean | Producer's Accuracy | User's Accuracy | F1 Score | Overall Accuracy |
|---|---|---|---|---|---|---|---|
| 2017 | Soybean | 679 | 352 | 65.86% | 72.47% | 0.69 | 77.08% |
|  | Non-Soybean | 258 | 1372 | 84.17% | 79.58% | 0.82 |  |
| 2018 | Soybean | 799 | 246 | 76.46% | 74.19% | 0.75 | 85.16% |
|  | Non-Soybean | 278 | 2208 | 88.82% | 89.98% | 0.89 |  |
| 2019* | Soybean | 1279 | 235 | 84.48% | 83.32% | 0.84 | 86.77% |
|  | Non-Soybean | 256 | 1940 | 88.34% | 89.20% | 0.89 |  |

382    * Including ground samples and nationwide reference points based on existing datasets.

**3.2 Spatial distributions of soybean planting areas**

384    Based on the soybean maps, we further analyzed the spatial patterns of soybean distribution in China

385    during 2017-2021. There were small changes in the spatial distribution of soybean in China in recent

386    years (Fig. 7-8). Several hot spots were obviously observed in Heilongjiang Province, eastern Inner

387    Mongolia, and northern Anhui, especially for eastern Inner Mongolia and western Heilongjiang,

388    extensively and densely distributed by soybean fields (Fig. 8b-c). In Region II, soybean was planted at a

389    larger scale, mainly concentrated in northern Anhui (Fig. 8d), and extensively distributed in Henan and

390    Shandong (Fig. 8e). Soybeans in other provinces of Region II, III, and IV were scattered distribution,

391    especially in the southwestern mountainous region (Fig. 8f-h).
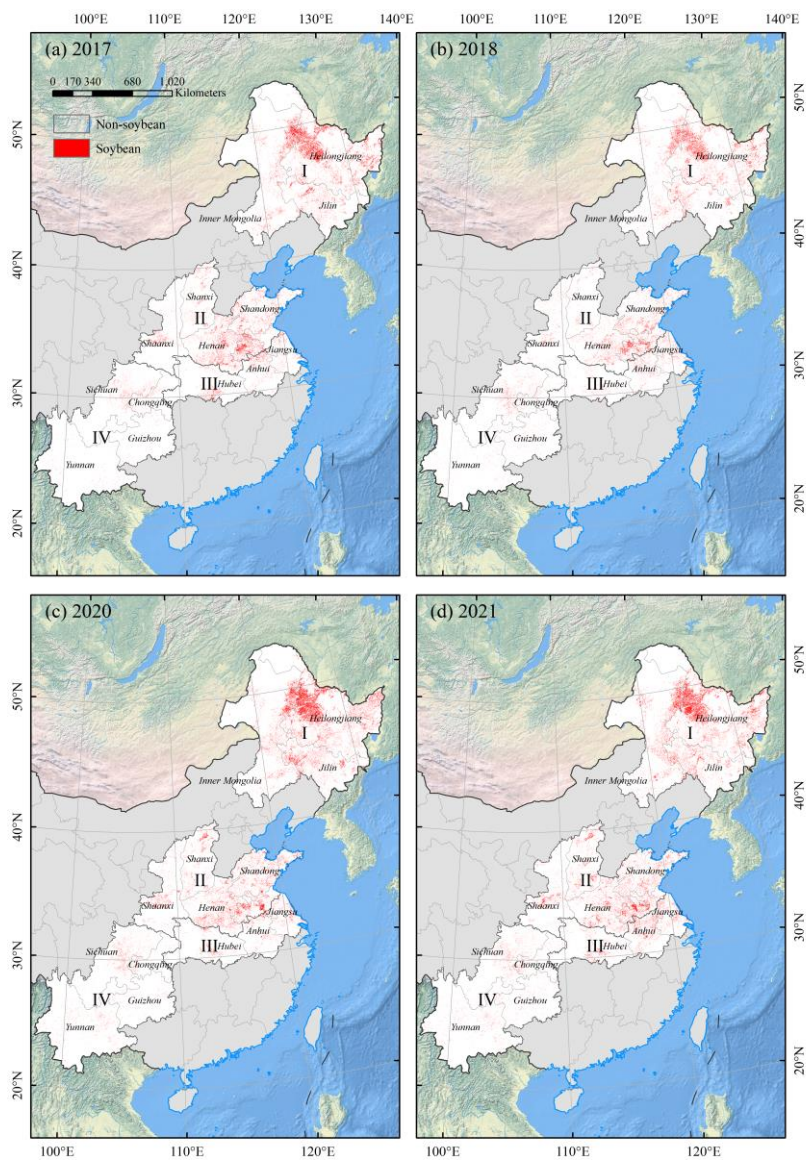
392

393    **Figure 7. Spatial distribution of soybean areas at 10 m resolution across China in (a) 2017, (b) 2018, (c) 2020**

394    **and (d) 2021.**

395
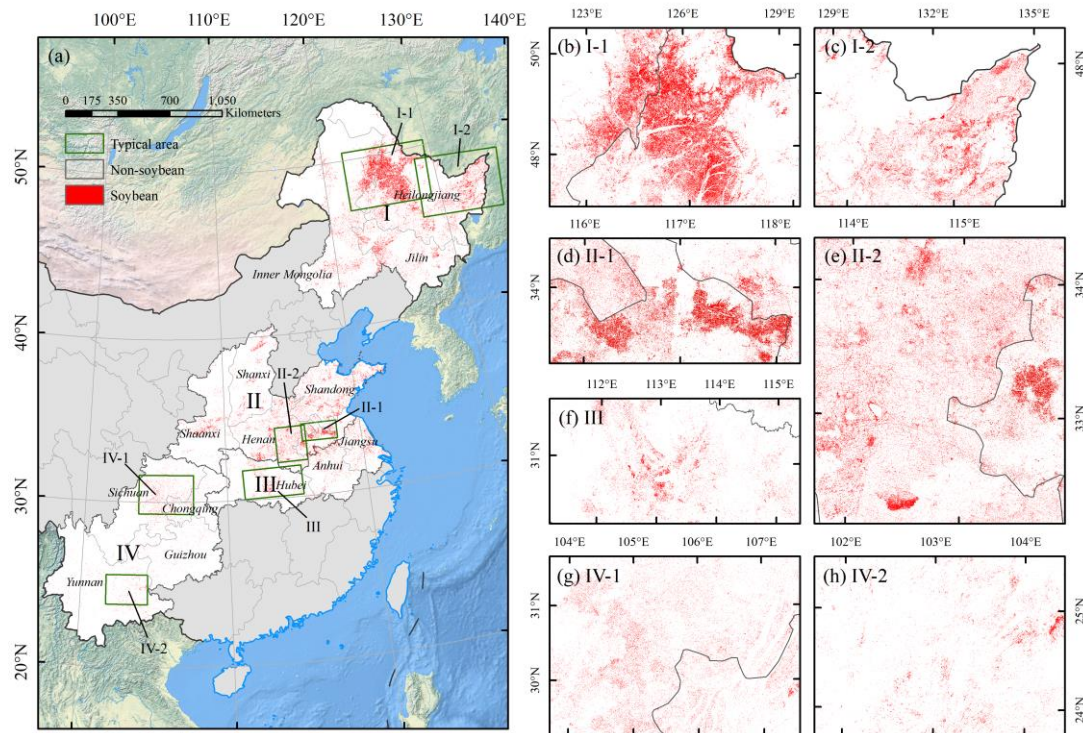
**Figure 8. Spatial distribution of soybean areas at 10 m resolution across China (a) and zoom-in maps of each**

**region (b-h) in 2019.**

To further compare soybean maps in detail, we compared ChinaSoyArea10m with GLAD maize-soybean map and CDL data products in space. The GLAD product is a 10-m resolution maize-soybean map of China in 2019, and their $R^2$ values with provincial and prefecture statistics were reported by 0.93 and 0.94 (Li et al., 2023). Arable land near waterbodies is often misclassified as soybean plots by CDL, which has not occurred by GLAD and ChinaSoyArea10m, implying other crop types are possibly misclassified as soybeans by CDL (Fig. 9 a1-d1). As for the second case (Fig. 9 a2), our extraction results are similar to those of GLAD, while small plots failed to be identified by CDL (Fig. 9 a2-d2). In areas where banded soybeans are planted less concentrated, CDL tended to overestimate the soybean area (Fig. 9 a3-d3), further substantiating the above limitations (Fig. 6). Conversely, our mapping results behaved similarly as GLAD did (Fig. 9 a3-d3). The overall accuracy of GLAD map based on pure samples reaches 95.4% (Li et al., 2023), so GLAD can be regarded as a reliable reference. From the three cases, therefore, ChinaSoyArea10m has behaved more similarly with GLAD than CDL does, indicated by less underestimation, less overestimation, and higher accuracy in details.
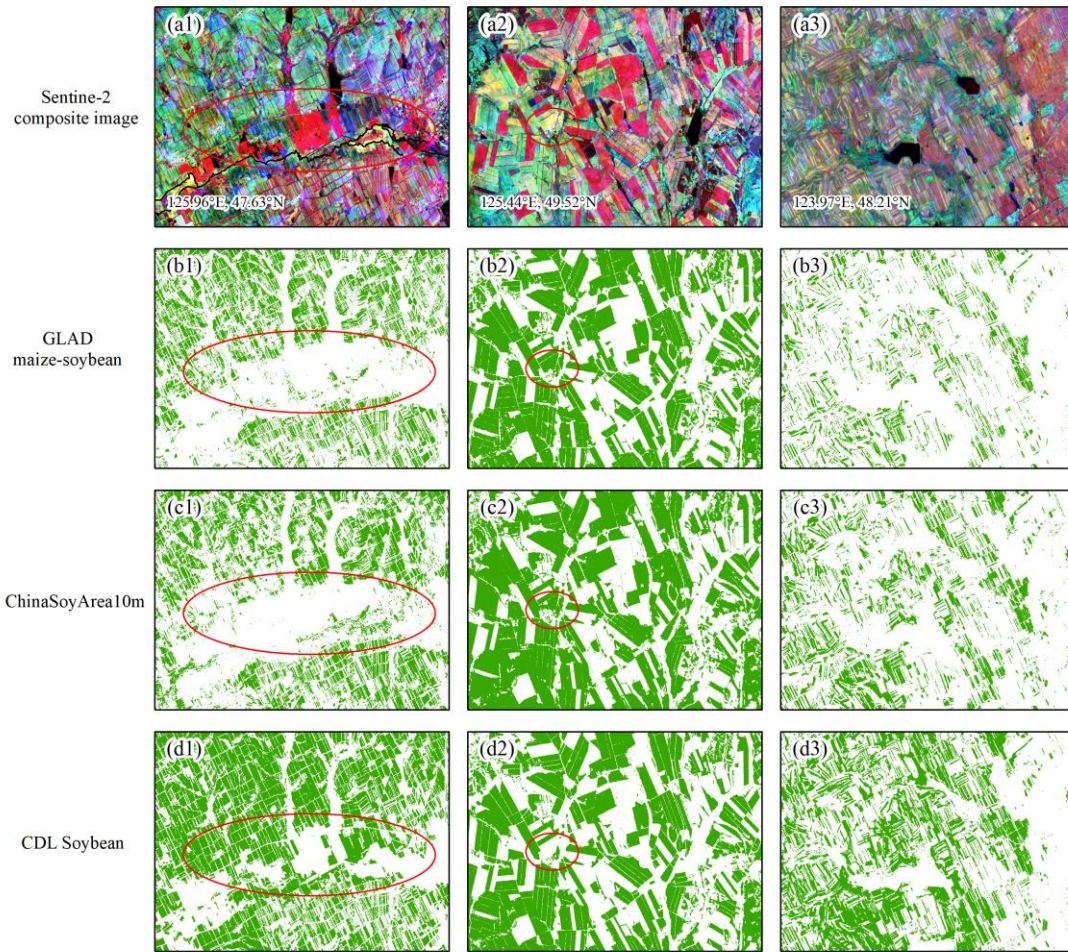
**Figure 9. Visual comparison of our soybean maps and existing products in typical regions in 2019: (a1-a3) RGB composite images comprise NIR (Band 8), SWIR 2 (Band 12), and SWIR 1 (Band 11) bands from Sentinel-2 median composite images during the peak growth period of soybean; (b1-b3) soybean layer extracted from GLAD maize-soybean map; (c1-c3) ChinaSoyArea10m map; (d1-d3) soybean layer extracted from CDL.**

**4 Discussion**

We proposed a new framework (RASP) to identify annual dynamic of soybean planting areas over larger regions. We produced the longer-term series of soybean maps (ChinaSoyArea10m) across mainly planting areas in China from 2017 to 2021 firstly. The accuracy of ChinaSoyArea10m is acceptable ($R^2 \sim 0.85$) at both county- and prefecture-level, relatively less than GLAD ($R^2 = 0.93$ at prefecture-level), but higher than CDL ($R^2 = 0.53$ at county-level). The RASP proposed does not require quantities of field samples and can self-adopt to different environments by considering

425     phenology information. Such an approach has its unique advantages, as well as some limitations.

426     **4.1 Our advantages and potential applicability**

427     The methodology developed for identifying soybean planting areas indicate several notable

428     strengths that make it an attractive option for wide application. Firstly, it operates independently,

429     without extensive ground samples required. The conventional approaches depend on quantities of

430     observational data, with much money, time, and labor consumed. In contrast, our strategy leverages

431     a specific, pre-existing set of samples to discern soybean characteristics, which can accurately map

432     annual dynamics without updated requirement in annual samples. Consequently, this method

433     significantly weakens limitations in crop classification during years without specific samples,

434     enabling crop mapping consistently and continually.

435     Another key advantage of our spectra-phenology integration approach is its quick applicability

436     over larger areas, coupled with excellent spatial scalability. The only inputs required are the

437     phenological information of soybeans and the number of other primary crops during the same

438     growing season in the targeted area. This allows to classify crop swiftly and efficiently without

439     additional inputs for background knowledge or setting complex thresholds. The input of

440     phenological information in each prefecture enhanced the zonal adaptive assessment of soybean

441     growth status across various areas, thereby facilitating crop classification. This innovative approach

442     ensures its applicability into other soybean-producing areas, showcasing its potential for broader

443     implementation.

444     **4.2 The uncertainty from image quality**

445     The method we proposed (RASP) is strongly dependent on remote sensing images and subregional

446     unsupervised classification by considering the bands and vegetation indices, which are all sensitive to

447     the unique characteristics of soybeans. Therefore, the accuracy of soybean maps inevitably is associated

448     with the quality of remote sensing images. By using ground samples to validate the mapping results, we

449     found that the accuracy of 2017 is lower than that of 2018 and 2019, with an overall accuracy is less than

450     80% (Table 2).

451     We extracted cloud-free images in different regions during the soybean growing season and calculated

452     the monthly average number of clear observations. In general, the monthly averages of clear observations

in Northeast region and Huang-Huai-Hai region (Zone I and Zone II) are relatively higher than the southern zones (Zone III and IV) (Fig. 10a2-e2). In areas with quite lower clear observations, despite a gap-filling method was conducted to generate complete 10-day composite time series, higher uncertainty is inevitable. The gap-filling time series might contain duplicate values, which cannot accurately reflect the crop growth process in reality. Obviously, the total number of images available in 2017 over the study areas was significantly fewer than those of other years (Fig.10a1-e1). Removing the cloudy pixels has left ever fewer clear images available (upper vs. down layer in Fig.10). During the growing season, the average number of clear observations per month was 0-2 in partial regions, lower than the requirements of 10-day time series composite we mentioned in 2.3.1. This might explain the lower user's accuracy of soybean in Zone IV compared to other sub-zones (Table S1) and low overall accuracy based on sample verification in 2017 (Table 2).
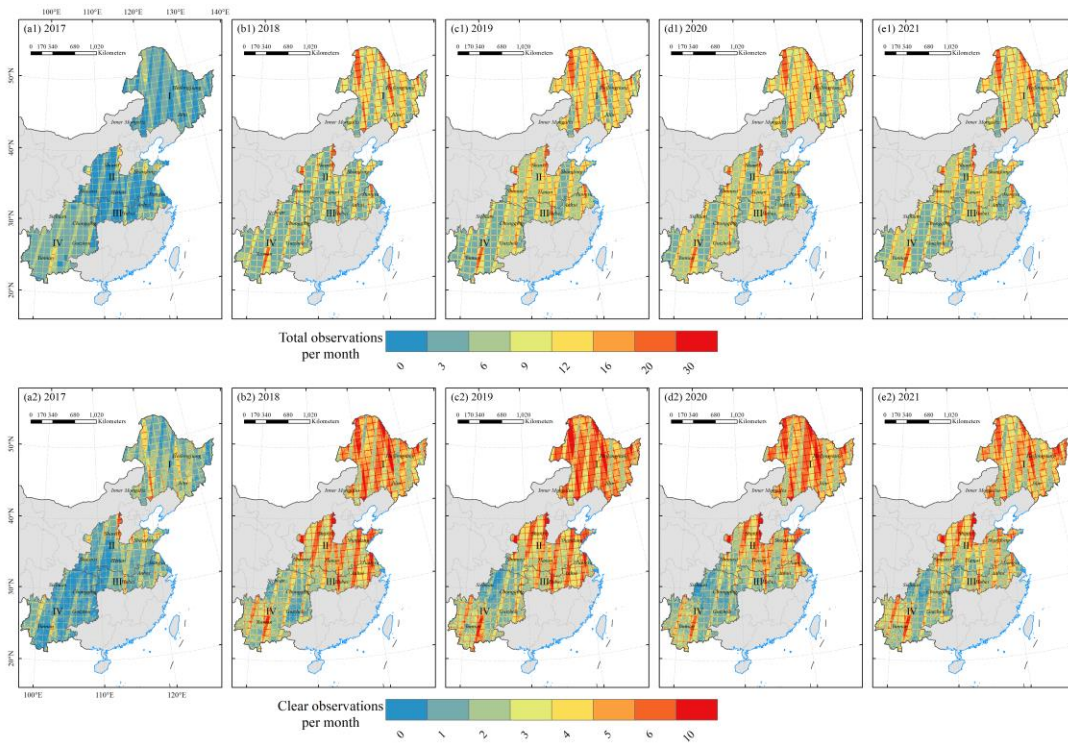
**Figure 10. Total (a1-e1) and clear (a2-e2) observations per month during soybean growing season.**

## 4.3 Limitations in small-scale planting areas

Validation based on statistics shows that ChinaSoyArea10m reached a high consistency ($R^2 \sim 0.85$) across China. However, in areas with soybean sparsely planted, the consistency is lower than that in densely planted areas, with more overestimations observed in the sparse areas. Such overestimations are caused

470 by the limitations of unsupervised classification algorithm. K-means is difficult to accurately capture

471 small plots of crops in a complex cropping system, although it can make up for the shortage of crop

472 mapping in some areas with limited training samples (Kwak and Park, 2022). Studies have proved that

473 the classifier performs inferiorly where dominant crop phenotypes are similar, and crop diversity is higher

474 (Wang et al., 2019; Konduri et al., 2020). Therefore, the classifier is challenged in areas where soybean

475 is not the dominant type due to the small plot size and spectral overlap between different crops (Chabalala

476 et al., 2022). In southern China, cropland plots are typically small (<0.04 ha in most regions) and the

477 crop diversity is high. The growth periods of soybean, peanut, potato, and maize are similar, dominantly

478 indicated by a mixed planting pattern, which has contributed to the low accuracy of non-main soybean

479 producing areas in southern China (Liu et al., 2020). Additionally, soybeans are intercropped with maize

480 or other crops in some areas, where the strip width is less one meter (Yang et al., 2014; Du et al., 2018).

481 This planting pattern will introduce the mixed pixels problem as well under the background of 10 m

482 resolution crop mapping.

483     The lower accuracy in soybean area sparely planted could be explained by the characteristics of K-

484 means algorithm. K-means algorithm is developed to minimize the distance between each point within a

485 cluster and the cluster's centroid. When the sample size in a particular category substantially exceeds

486 those of others, the algorithm might preferentially optimize the cohesion of the larger category, and would

487 neglect the accurate clustering for smaller categories (Tan et al., 2016). The effectiveness of K-means

488 classification is highly dependent on the selection of initial clustering centers. In scenarios of unbalanced

489 categories, initial centers randomly selected might inadequately represent the minor categories, resulting

490 in inaccurate results (Tan et al., 2016). Additionally, K-means assumes that each cluster is spherical;

491 therefore, it does not perform well when clusters are non-spherical and uneven in size and density. Hence,

492 in areas with unbalanced crop categories, the algorithm faces challenge to assign each crop to a

493 corresponding cluster precisely (Tan et al., 2016; Wang et al., 2019).

494     Our regional adaptive large-area crop mapping method in future will further be improved by the

495 follows: (1) Classification on a finer scale by specifying a more precise number of target clusters can

496 reduce spatial heterogeneity and emphasize the relative importance of non-dominant categories, and

497 increase classification accuracy consequently (Li and Yang, 2017). (2) Optimizing data preprocessing

498 methods. Outliers can interrupt classification because the unsupervised methods is highly sensitive to

anomalies (Raykov et al., 2016; Wang et al., 2019). Therefore, eliminating outliers can further improve the classification validity. In addition, since K-means weights all dimensions equally, minimizing the features' correlation and reducing irrelevant variables are also important means to enhance the classification effect (Hastie et al., 2009). (3) Improving algorithm performance. A variety of algorithms have been proposed to address the inherent defects of K-means (Ahmed et al., 2020), such as by optimizing the initial clustering center (e.g., K-means++), weighting classes (e.g., Weighted k-means), and non-spherical clustering assumptions (e.g., DBSCAN, Spectral Clustering) (Ester et al., 1996; Bach and Jordan, 2003; Kerdprasop et al., 2005; Arthur and Vassilvitskii, 2007). The improved algorithms will address the issues on complex and highly diverse crop classification in some degrees (Li et al., 2022; Rivera et al., 2022). (4) Better post-processing of data. Misclassification of field ridges and image speckles is inevitable during mapping crops over large areas. With the progress of computing power, auxiliary data and image processing algorithms can further eliminate these issues (Liu et al., 2018a; Li and Qu, 2019; Hamano et al., 2023). We are sure that integrating cloud computing platforms with advanced algorithms will provide substantial potential for accurate crop identification covering larger areas in future.

## 5 Data availability

The soybean planting area product for China during 2017-2021 (ChinaSoyArea10m) is available at https://zenodo.org/doi/10.5281/zenodo.10071426 (Mei et al., 2023). We encourage users to independently verify data products for special study areas before using them.

## 6 Conclusions

In this study, a Reginal Adaption Spectra-Phenology Integration (RASP) method over large-scale was developed and utilized to generate soybean planting area maps for major producing regions in China from 2017 to 2021. By utilizing Sentinel-2 images, spectral features and vegetation indices that best distinguish soybeans were extracted and input into an unsupervised classifier in each prefecture. The DTW method was then employed to identify the soybean distribution. RASP does not rely on many ground samples and considers the soybean phenology in various planting areas, suggesting a potential

way for long-term crop mapping over larger regions. Verification results demonstrated a high consistency between the mapping results and census data at county or prefecture level (all > 0.82), with overall accuracies of field samples reaching 77.08%~86.77%. These findings confirm the reliability of ChinaSoyArea10m. Our data products fill the gap in regional long-term soybean maps in China, and provide important information for sustainable soybean production and management, agricultural system modeling, and optimization.

**Author contributions.**

ZZ and FT conceive this study. QM, JH, and JD collected datasets. QM implemented the research and wrote the original draft of the paper. All authors discussed the results and revised the manuscript.

**Competing interests.**

The contact author has declared that neither they nor their co-authors have any competing interests.

**Financial support.**

This research was funded by the National Key Research and Development Program of China (2020YFA0608201) and National Natural Science Foundation of China (42061144003, 41977405).

**References**

Ahmed, M., Seraj, R., and Islam, S. M. S.: The k-means Algorithm: A Comprehensive Survey and Performance Evaluation, Electronics, 9, 1295, https://doi.org/10.3390/electronics9081295, 2020.

FAOSTAT: https://www.fao.org/faostat/en/#rankings/countries_by_commodity, last access: 10 October 2023.

National Bureau of Statistics of China: http://www.stats.gov.cn/english/, last access: 23 October 2023.

Arthur, D. and Vassilvitskii, S.: k-means++: The advantages of careful seeding, in: Soda, 1027–1035, 2007.

547 Bach, F. and Jordan, M.: Learning spectral clustering, in: Advances in neural information processing

548 systems, 2003.

549 Chabalala, Y., Adam, E., and Ali, K. A.: Machine Learning Classification of Fused Sentinel-1 and

550 Sentinel-2 Image Data towards Mapping Fruit Plantations in Highly Heterogenous Landscapes, Remote

551 Sens., 14, 2621, https://doi.org/10.3390/rs14112621, 2022.

552 Chen, D., Huang, J., and Jackson, T. J.: Vegetation water content estimation for corn and soybeans using

553 spectral indices derived from MODIS near- and short-wave infrared bands, Remote Sens. Environ., 98,

554 225–236, https://doi.org/10.1016/j.rse.2005.07.008, 2005.

555 Chen, H., Li, H., Liu, Z., Zhang, C., Zhang, S., and Atkinson, P. M.: A novel Greenness and Water Content

556 Composite Index (GWCCI) for soybean mapping from single remotely sensed multispectral images,

557 Remote Sens. Environ., 295, 113679, https://doi.org/10.1016/j.rse.2023.113679, 2023.

558 Cui, K. and Shoemaker, S. P.: A look at food security in China, npj Sci. Food, 2, 4,

559 https://doi.org/10.1038/s41538-018-0012-x, 2018.

560 Di Tommaso, S., Wang, S., and Lobell, D. B.: Combining GEDI and Sentinel-2 for wall-to-wall mapping

561 of tall and short crops, Environ. Res. Lett., 16, 125002, https://doi.org/10.1088/1748-9326/ac358c, 2021.

562 Dong, J., Fu, Y., Wang, J., Tian, H., Fu, S., Niu, Z., Han, W., Zheng, Y., Huang, J., and Yuan, W.: Early-

563 season mapping of winter wheat in China based on Landsat and Sentinel images, Earth Syst. Sci. Data,

564 12, 3081–3095, https://doi.org/10.5194/essd-12-3081-2020, 2020.

565 Du, J., Han, T., Gai, J., Yong, T., Sun, X., Wang, X., Yang, F., Liu, J., Shu, K., Liu, W., and Yang, W.:

566 Maize-soybean strip intercropping: Achieved a balance between high productivity and sustainability, J.

567 Integr. Agric., 17, 747–754, https://doi.org/10.1016/S2095-3119(17)61789-1, 2018.

568 Ester, M., Kriegel, H.-P., Sander, J., and Xu, X.: A density-based algorithm for discovering clusters in

569 large spatial databases with noise, in: kdd, 226–231, 1996.

570 Fensholt, R. and Sandholt, I.: Derivation of a shortwave infrared water stress index from MODIS near-

571 and shortwave infrared data in a semiarid environment, Remote Sens. Environ., 87, 111–121,

572 https://doi.org/10.1016/j.rse.2003.07.002, 2003.

573 Gong, L., Tian, B., Li, Y., and Wu, S.: Phenological Changes of Soybean in Response to Climate

574 Conditions in Frigid Region in China over the Past Decades, Int. J. Plant Prod., 15, 363–375,

575 https://doi.org/10.1007/s42106-021-00145-5, 2021.

576 Graesser, J. and Ramankutty, N.: Detection of cropland field parcels from Landsat imagery, Remote Sens.

577 Environ., 201, 165–180, https://doi.org/10.1016/j.rse.2017.08.027, 2017.

578 Guan, X., Huang, C., Liu, G., Meng, X., and Liu, Q.: Mapping Rice Cropping Systems in Vietnam Using

579 an NDVI-Based Time-Series Similarity Measurement Based on DTW Distance, Remote Sens., 8, 19,

580 https://doi.org/10.3390/rs8010019, 2016.

581 Guo, W., Ren, J., Liu, X., Chen, Z., Wu, S., and Pan, H.: Winter wheat mapping with globally optimized

582 threshold under total quantity constraint of statistical data, J. Remote Sens., 22, 1023–1041,

583 https://doi.org/10.11834/jrs.20187468, 2018.

584 Hamano, M., Shiozawa, S., Yamamoto, S., Suzuki, N., Kitaki, Y., and Watanabe, O.: Development of a

585 method for detecting the planting and ridge areas in paddy fields using AI, GIS, and precise DEM,

586 Precision Agric, 24, 1862–1888, https://doi.org/10.1007/s11119-023-10021-z, 2023.

587 Han, J., Zhang, Z., Luo, Y., Cao, J., Zhang, L., Zhang, J., and Li, Z.: The RapeseedMap10 database:

588 annual maps of rapeseed at a spatial resolution of 10 m based on multi-source data, Earth Syst. Sci. Data,

589 13, 2857–2874, https://doi.org/10.5194/essd-13-2857-2021, 2021.

590 Han, J., Zhang, Z., Luo, Y., Cao, J., Zhang, L., Zhuang, H., Cheng, F., Zhang, J., and Tao, F.: Annual

591 paddy rice planting area and cropping intensity datasets and their dynamics in the Asian monsoon region

592 from 2000 to 2020, Agric. Syst., 200, 103437, https://doi.org/10.1016/j.agsy.2022.103437, 2022.

593 Hartman, G. L., West, E. D., and Herman, T. K.: Crops that feed the World 2. Soybean—worldwide

594 production, use, and constraints caused by pathogens and pests, Food Secur., 3, 5–17,

595 https://doi.org/10.1007/s12571-010-0108-x, 2011.

596 Hastie, T., Tibshirani, R., Friedman, J. H., and Friedman, J. H.: The elements of statistical learning: data

597 mining, inference, and prediction, Springer, 2009.

598 Housman, I. W., Chastain, R. A., and Finco, M. V.: An Evaluation of Forest Health Insect and Disease

599 Survey Data and Satellite-Based Remote Sensing Forest Change Detection Methods: Case Studies in the

600 United States, Remote Sens., 10, 1184, https://doi.org/10.3390/rs10081184, 2018.

601 Huang, Y., Qiu, B., Chen, C., Zhu, X., Wu, W., Jiang, F., Lin, D., and Peng, Y.: Automated soybean

602 mapping based on canopy water content and chlorophyll content using Sentinel-2 images, Int. J. Appl.

603 Earth Obs., 109, 102801, https://doi.org/10.1016/j.jag.2022.102801, 2022.

604 Kerdprasop, K., Kerdprasop, N., and Sattayatham, P.: Weighted k-means for density-biased clustering,

in: International conference on data warehousing and knowledge discovery, 488–497, https://doi.org/10.1007/11546849_48, 2005.

Konduri, V. S., Kumar, J., Hargrove, W. W., Hoffman, F. M., and Ganguly, A. R.: Mapping crops within the growing season across the United States, Remote Sens. Environ., 251, 112048, https://doi.org/10.1016/j.rse.2020.112048, 2020.

Kumari, M., Murthy, C. S., Pandey, V., and Bairagi, G. D.: Soybean Cropland Mapping Using Multi-Temporal Sentinel-1 Data, Int. Arch. Photogramm. Remote Sens. Spat. Inf. Sci., XLII-3-W6, 109–114, https://doi.org/10.5194/isprs-archives-XLII-3-W6-109-2019, 2019.

Kwak, G.-H. and Park, N.-W.: Unsupervised Domain Adaptation with Adversarial Self-Training for Crop Classification Using Remote Sensing Images, Remote Sens., 14, 4639, https://doi.org/10.3390/rs14184639, 2022.

Li, B. and Yang, L.: Clustering accuracy analysis of building area in high spatial resolution remote sensing images based on k-means algorithm, in: 2017 2nd International Conference on Frontiers of Sensors Technologies (ICFST), 2017 2nd International Conference on Frontiers of Sensors Technologies (ICFST), 174–178, https://doi.org/10.1109/ICFST.2017.8210497, 2017.

Li, H., Song, X.-P., Hansen, M. C., Becker-Reshef, I., Adusei, B., Pickering, J., Wang, L., Wang, L., Lin, Z., Zalles, V., Potapov, P., Stehman, S. V., and Justice, C.: Development of a 10-m resolution maize and soybean map over China: Matching satellite-based crop classification with sample-based area estimation, Remote Sens. Environ., 294, 113623, https://doi.org/10.1016/j.rse.2023.113623, 2023.

Li, L., Friedl, M. A., Xin, Q., Gray, J., Pan, Y., and Frolking, S.: Mapping Crop Cycles in China Using MODIS-EVI Time Series, Remote Sens., 6, 2473–2493, https://doi.org/10.3390/rs6032473, 2014.

Li, T., Johansen, K., and McCabe, M. F.: A machine learning approach for identifying and delineating agricultural fields and their multi-temporal dynamics using three decades of Landsat data, ISPRS J. Photogramm. Remote Sens., 186, 83–101, https://doi.org/10.1016/j.isprsjprs.2022.02.002, 2022.

Li, Y. and Qu, H.: LSD and Skeleton Extraction Combined with Farmland Ridge Detection, in: Advances in Intelligent, Interactive Systems and Applications, Cham, 446–453, https://doi.org/10.1007/978-3-030-02804-6_59, 2019.

Liu, H., Zhang, J., Pan, Y., Shuai, G., Zhu, X., and Zhu, S.: An Efficient Approach Based on UAV Orthographic Imagery to Map Paddy With Support of Field-Level Canopy Height From Point Cloud

Data, IEEE J. Sel. Top. Appl. Earth Obs. Remote Sens., 11, 2034–2046, https://doi.org/10.1109/JSTARS.2018.2829218, 2018a.

Liu, J., Wang, L., Yang, F., Yao, B., and Yang, L.: Recognition ability of red edge and short wave infrared spectrum on maize and soybean, Chinese Agricultural Science Bulletin, 34, 120–129, 2018b.

Liu, L., Xiao, X., Qin, Y., Wang, J., Xu, X., Hu, Y., and Qiao, Z.: Mapping cropping intensity in China using time series Landsat and Sentinel-2 images and Google Earth Engine, Remote Sens. Environ., 239, 111624, https://doi.org/10.1016/j.rse.2019.111624, 2020.

Liu, M. and Fan, Q.: Study on the Current Situation and Problems of Soybean Consumption, Production and Import in China, Grain Science And Technology And Economy, 46, 28–35, https://doi.org/10.16465/j.gste.cn431252ts.20210606, 2021.

Liu, Z., Ying, H., Chen, M., Bai, J., Xue, Y., Yin, Y., Batchelor, W. D., Yang, Y., Bai, Z., Du, M., Guo, Y., Zhang, Q., Cui, Z., Zhang, F., and Dou, Z.: Optimization of China's maize and soy production can ensure feed sufficiency at lower nitrogen and carbon footprints, Nat. Food, 2, 426–433, https://doi.org/10.1038/s43016-021-00300-1, 2021.

Lowder, S. K., Skoet, J., and Raney, T.: The Number, Size, and Distribution of Farms, Smallholder Farms, and Family Farms Worldwide, World Dev., 87, 16–29, https://doi.org/10.1016/j.worlddev.2015.10.041, 2016.

Luo, C., Liu, H., Lu, L., Liu, Z., Kong, F., and Zhang, X.: Monthly composites from Sentinel-1 and Sentinel-2 images for regional major crop mapping with Google Earth Engine, J. Integr. Agr., 20, 1944–1957, https://doi.org/10.1016/S2095-3119(20)63329-9, 2021.

Luo, Y., Zhang, Z., Li, Z., Chen, Y., Zhang, L., Cao, J., and Tao, F.: Identifying the spatiotemporal changes of annual harvesting areas for three staple crops in China by integrating multi-data sources, Environ. Res. Lett., 15, 074003, https://doi.org/10.1088/1748-9326/ab80f0, 2020.

Luo, Y., Zhang, Z., Zhang, L., Han, J., Cao, J., and Zhang, J.: Developing High-Resolution Crop Maps for Major Crops in the European Union Based on Transductive Transfer Learning and Limited Ground Data, Remote Sens., 14, 1809, https://doi.org/10.3390/rs14081809, 2022.

Ma, Z., Liu, Z., Zhao, Y., Zhang, L., Liu, D., Ren, T., Zhang, X., and Li, S.: An Unsupervised Crop Classification Method Based on Principal Components Isometric Binning, ISPRS Int. J. Geo-Inf., 9, 648, https://doi.org/10.3390/ijgi9110648, 2020.

663 Marshall, M., Belgiu, M., Boschetti, M., Pepe, M., Stein, A., and Nelson, A.: Field-level crop yield

664 estimation with PRISMA and Sentinel-2, ISPRS J. Photogramm. Remote Sens., 187, 191–210,

665 https://doi.org/10.1016/j.isprsjprs.2022.03.008, 2022.

666 Mei, Q., Zhang, Z., Han, J., Song, J., Dong, J., Wu, H., Xu, J., and Tao, F.: ChinaSoyArea10m: a dataset

667 of soybean planting areas with a spatial resolution of 10 m across China from 2017 to 2021 (V1), Zenodo

668 [data set], https://doi.org/10.5281/zenodo.10071427, 2023.

669 Olsen, J. L., Stisen, S., Proud, S. R., and Fensholt, R.: Evaluating EO-based canopy water stress from

670 seasonally detrended NDVI and SIWSI with modeled evapotranspiration in the Senegal River Basin,

671 Remote Sens. Environ., 159, 57–69, https://doi.org/10.1016/j.rse.2014.11.029, 2015.

672 Oreopoulos, L., Wilson, M. J., and Várnai, T.: Implementation on Landsat Data of a Simple Cloud-Mask

673 Algorithm Developed for MODIS Land Bands, IEEE Geosci. Remote. Sens. Lett., 8, 597–601,

674 https://doi.org/10.1109/LGRS.2010.2095409, 2011.

675 Pan, B., Zheng, Y., Shen, R., Ye, T., Zhao, W., Dong, J., Ma, H., and Yuan, W.: High Resolution

676 Distribution Dataset of Double-Season Paddy Rice in China, Remote Sens., 13, 4609,

677 https://doi.org/10.3390/rs13224609, 2021.

678 Potapov, P., Turubanova, S., Hansen, M. C., Tyukavina, A., Zalles, V., Khan, A., Song, X.-P., Pickens, A.,

679 Shen, Q., and Cortez, J.: Global maps of cropland extent and change show accelerated cropland

680 expansion in the twenty-first century, Nat. Food, 3, 19–28, https://doi.org/10.1038/s43016-021-00429-z,

681 2022.

682 Raykov Y. P., Boukouvalas A., Baig F., and Little M. A.: What to Do When K-Means Clustering Fails: A

683 Simple yet Principled Alternative Algorithm, PLOS ONE, 11, e0162259,

684 https://doi.org/10.1371/journal.pone.0162259, 2016.

685 Rivera, A. J., Pérez-Godoy, M. D., Elizondo, D., Deka, L., and del Jesus, M. J.: Analysis of clustering

686 methods for crop type mapping using satellite imagery, Neurocomputing, 492, 91–106,

687 https://doi.org/10.1016/j.neucom.2022.04.002, 2022.

688 Shangguan, Y., Li, X., Lin, Y., Deng, J., and Yu, L.: Mapping spatial-temporal nationwide soybean

689 planting area in Argentina using Google Earth Engine, Int. J. Remote Sens., 43, 1724–1748,

690 https://doi.org/10.1080/01431161.2022.2049913, 2022.

691 Shen, R., Dong, J., Yuan, W., Han, W., Ye, T., and Zhao, W.: A 30 m Resolution Distribution Map of

Maize for China Based on Landsat and Sentinel Images, J. Remote Sens., 2022, 2022/9846712, https://doi.org/10.34133/2022/9846712, 2022.

Shen, R., Pan, B., Peng, Q., Dong, J., Chen, X., Zhang, X., Ye, T., Huang, J., and Yuan, W.: High-resolution distribution maps of single-season rice in China from 2017 to 2022, Earth Syst. Sci. Data, 15, 3203–3222, https://doi.org/10.5194/essd-15-3203-2023, 2023.

Sobejano-Paz, V., Mikkelsen, T. N., Baum, A., Mo, X., Liu, S., Köppl, C. J., Johnson, M. S., Gulyas, L., and García, M.: Hyperspectral and Thermal Sensing of Stomatal Conductance, Transpiration, and Photosynthesis for Soybean and Maize under Drought, Remote Sens., 12, 3182, https://doi.org/10.3390/rs12193182, 2020.

Song, X.-P., Potapov, P. V., Krylov, A., King, L., Di Bella, C. M., Hudson, A., Khan, A., Adusei, B., Stehman, S. V., and Hansen, M. C.: National-scale soybean mapping and area estimation in the United States using medium resolution satellite imagery and field survey, Remote Sens. Environ., 190, 383–395, https://doi.org/10.1016/j.rse.2017.01.008, 2017.

Tan, P.-N., Steinbach, M., and Kumar, V.: Introduction to data mining, Pearson Education India, 2016.

Wang, S., Azzari, G., and Lobell, D. B.: Crop type mapping without field-level labels: Random forest transfer and unsupervised clustering techniques, Remote Sens. Environ., 222, 303–317, https://doi.org/10.1016/j.rse.2018.12.026, 2019.

Wang, S., Di Tommaso, S., Deines, J. M., and Lobell, D. B.: Mapping twenty years of corn and soybean across the US Midwest using the Landsat archive, Sci. Data, 7, 307, https://doi.org/10.1038/s41597-020-00646-4, 2020.

Wang, Y. and Gai, J.: Study on the ecological regions of soybean in China II · Ecological environment and representative varieties, Chinese Journal of Applied Ecology, 71–75, 2002.

Wang, Y., Feng, L., Sun, W., Zhang, Z., Zhang, H., Yang, G., and Meng, X.: Exploring the potential of multi-source unsupervised domain adaptation in crop mapping using Sentinel-2 images, Gisci. Remote Sens., 59, 2247–2265, https://doi.org/10.1080/15481603.2022.2156123, 2022.

Wang, Y., Ling, X., Ma, C., Liu, C., Zhang, W., Huang, J., Peng, S., and Deng, N.: Can China get out of soy dilemma? A yield gap analysis of soybean in China, Agron. Sustain. Dev., 43, 47, https://doi.org/10.1007/s13593-023-00897-6, 2023.

Xiong, J., Thenkabail, P. S., Gumma, M. K., Teluguntla, P., Poehnelt, J., Congalton, R. G., Yadav, K.,

721  and Thau, D.: Automated cropland mapping of continental Africa using Google Earth Engine cloud

722  computing, ISPRS J. Photogramm. Remote Sens., 126, 225–244,

723  https://doi.org/10.1016/j.isprsjprs.2017.01.019, 2017.

724  Yang, F., Huang, S., Gao, R., Liu, W., Yong, T., Wang, X., Wu, X., and Yang, W.: Growth of soybean

725  seedlings in relay strip intercropping systems in relation to light quantity and red:far-red ratio, Field

726  Crops Res., 155, 245–253, https://doi.org/10.1016/j.fcr.2013.08.011, 2014.

727  You, N. and Dong, J.: Examining earliest identifiable timing of crops using all available Sentinel 1/2

728  imagery and Google Earth Engine, ISPRS J. Photogramm. Remote Sens., 161, 109–123,

729  https://doi.org/10.1016/j.isprsjprs.2020.01.001, 2020.

730  You, N., Dong, J., Huang, J., Du, G., Zhang, G., He, Y., Yang, T., Di, Y., and Xiao, X.: The 10-m crop

731  type maps in Northeast China during 2017–2019, Sci. Data, 8, 41, https://doi.org/10.1038/s41597-021-

732  00827-9, 2021.

733  You, N., Dong, J., Li, J., Huang, J., and Jin, Z.: Rapid early-season maize mapping without crop labels,

734  Remote Sens. Environ., 290, 113496, https://doi.org/10.1016/j.rse.2023.113496, 2023.

735  Zhang, C., Dong, J., and Ge, Q.: Quantifying the accuracies of six 30-m cropland datasets over China: A

736  comparison and evaluation analysis, Comput. Electron. Agr., 197, 106946,

737  https://doi.org/10.1016/j.compag.2022.106946, 2022.

738  Zhang, G., Xiao, X., Biradar, C. M., Dong, J., Qin, Y., Menarguez, M. A., Zhou, Y., Zhang, Y., Jin, C.,

739  Wang, J., Doughty, R. B., Ding, M., and Moore, B.: Spatiotemporal patterns of paddy rice croplands in

740  China and India from 2000 to 2015, Sci. Total Environ., 579, 82–92,

741  https://doi.org/10.1016/j.scitotenv.2016.10.223, 2017.

742  Zhong, L., Hu, L., Yu, L., Gong, P., and Biging, G. S.: Automated mapping of soybean and corn using

743  phenology, ISPRS J. Photogramm. Remote Sens., 119, 151–164,

744  https://doi.org/10.1016/j.isprsjprs.2016.05.014, 2016.

745  Zhou, W., Wei, H., Chen, Y., Zhang, X., Hu, J., Cai, Z., Yang, J., Hu, Q., Xiong, H., Yin, G., and Xu, B.:

746  Monitoring intra-annual and interannual variability in spatial distribution of plastic-mulched citrus in

747  cloudy and rainy areas using multisource remote sensing data, Eur. J. Agron., 151, 126981,

748  https://doi.org/10.1016/j.eja.2023.126981, 2023.

749